PREPARATION OF Au-Pt NANOSTRUCTURES ON HIGHLY ORIENTED PYROLYTIC GRAPHITE SURFACES BY PULSED LASER DEPOSITION AND THEIR CHARACTERIZATION BY XPS AND AFM METHODS

Jan PLŠEK[1], Pavel JANDA[2] and Zdeněk BASTL[3,*]

J. Heyrovský Institute of Physical Chemistry, Academy of Sciences of the Czech Republic, v.v.i., Dolejškova 3, 182 23 Prague 8, Czech Republic; e-mail: [1] plsek@jh-inst.cas.cz, [2] janda@jh-inst.cas.cz, [3] bastl@jh-inst.cas.cz

Received May 13, 2008
Accepted August 18, 2008
Published online November 27, 2008

Dedicated to Professor Rudolf Zahradník on the occasion of his 80th birthday.

Au-Pt nanostructures on highly oriented pyrolytic graphite (HOPG) were prepared by irradiating bimetallic target under ultrahigh vacuum with pulsed radiation of Nd:YAG laser. The deposited nanostructures were characterized by X-ray photoelectron spectroscopy (XPS) and atomic force microscopy (AFM). The measured spectra of Au (4f) and Pt (4f) photoelectrons of laser deposits were composed of two overlapping doublets. Analysis of images obtained from AFM revealed bimodal particle size distribution and presence of few large particles. In agreement with AFM images of the deposit we attributed a two doublet structure of Au (4f) and Pt (4f) spectra to bimodal nanoparticle size distribution. Carbon KLL Auger electron spectra revealed formation of defects in the superficial layers of HOPG by impinging metal ions accompanied by appearance of sp^3 hybridized carbon atoms. The dependence of Au (4f) and Pt (4f) core level binding energies on the amount of metals deposited and formation of bimetallic nanoparticles are discussed.

Keywords: Au-Pt; Bimetallic nanostructures; Graphite; Pulsed laser deposition; X-ray photoelectron spectroscopy; AFM.

Supported metallic and bimetallic nanoparticles have attracted considerable fundamental and practical interests in heterogeneous and fuel cell catalysis because of their unique catalytic properties[1,2]. Recently, increasing number of extensive studies have been reported on application of gold based nanoparticles[3,4]. Oxide-supported gold nanoparticles were found to be one of the best catalysts for low temperature CO oxidation[3–6]. Modern catalysts are often bimetallic. They frequently contain an active metal combined with a less active metal. The role of the second metal is to enhance catalyst performance by electronic or ligand effect or by preventing undesired reac-

doi:10.1135/cccc20081299

tions. It is well known that activity and selectivity of supported bimetallic catalysts is influenced by structure and composition of their surface, size of the nanoparticles, their electronic structure and interaction with supporting material.

Supported bimetallic Au-Pt nanoparticles are of great interest as dehydrogenation catalysts and electrocatalysts in oxidation of various alcohols under mild conditions[7–10] and reduction of oxygen[11]. The origin of catalytic properties of this catalyst is not yet fully understood. It has been recently suggested that Au-Pt nanoparticles provide synergistic catalytic effects consisting in the suppression of adsorption of poisonous species (e.g. carbon monoxide) and the change in electronic structure modifying the strength of adsorption[10]. The desorption temperature of CO on Pt-Au alloy surface was found to depend linearly on the concentration of surface Au atoms[12]. Recent density functional theory (DFT) calculations have indicated that the change in the bonding energy of CO molecule to alloy surface is proportional to the shift of the d-band centre of gravity[13]. The catalytic properties of supported Au-Pt catalyst prepared by impregnation were observed to be similar to that of monometallic Pt catalyst[14]. This finding was explained by phase separation of the two metals due to miscibility gap in a wide composition range[2]. On the other hand, recent X-ray diffraction studies of the Au-Pt particles prepared by molecular capping based colloidal synthesis and subsequently deposited on carbon support have shown that after thermal treatment[15] alloy phase is present in contrast to miscibility gap. It has also been demonstrated that heat of formation of alloy particles exhibits size dependence and the metals immiscible in bulk can form alloy nanoparticles[16].

Wet impregnation methods usually used for preparation of laboratory and industrial supported bimetallic catalysts result in ill-defined and contaminated particles which are not suitable for study by modern surface selective experimental methods. Beside it, the size and composition of individual metallic particles in catalysts prepared by wet methods widely vary within a given sample. This inhomogeneity complicates significantly understanding of their catalytic properties. Various methods were suggested to fabricate well-defined model catalysts. Bimetallic cluster compounds were used as catalyst precursors[17,18] but the metals and metal ratios can not be simply varied in this method. Thermal decomposition of dendrimer encapsulated metals can also be used for preparation of bimetallic catalysts[19]. Using the dendrimer method homogeneous and monodispersed nanoparticles with well defined and reproducible composition can be prepared. Bimetallic nanoparticles consisting of Au-Pt, Au-Pd and Au-Ag were synthe-

sized by a sol-gel process[20]. Au-Pt colloidal particles were also prepared by a rapid butyllithium reduction of Au^{3+} and Pt^{4+} precursors[21].

Evaporation of a metal in ultrahigh vacuum on well defined substrate is often used as relatively simple method for preparation of supported metal particles. Unfortunately, the resulting particles are usually not uniform in size. Consecutive vacuum deposition of Pd and Au metals on oxide layer grown on $Ni_3Al(111)$ surface was reported as a method for bimetallic model catalyst preparation[22]. In this method Pd atoms first nucleate on point defects of the oxide film and form there clusters which in the next step act as nucleation centres for Au atoms. Using similar approach the authors[23] prepared Co-Pd nanoparticles on alumina film grown on NiAl(110) substrate.

The pulsed laser deposition (PLD) is a new technique in the field of preparation of mono- and multimetallic supported nanoparticles for catalytic applications[24–29]. In this technique the laser pulses are focused on the solid target and evaporate material from its surface. The ejected particles condense on the support surface. The target composition can be varied to achieve the required composition of the deposit. The sizes of nanoparticles can be adjusted and supported nanoparticles with narrow size distribution can be prepared. Stoichiometry of the target can be reproduced in the deposited material provided the laser fluence is higher than a threshold value. The fluence can be increased by increasing the pulse energy or by decreasing the size of the laser spot on the target surface until the value required is achieved. In spite of fact that PLD received extensive development and is used for preparation of various kinds of nanomaterials the growth process of nanostructures by PLD is rather complex and not fully understood.

The aim of this study is to prepare supported Au-Pt nanoparticles from bulk bimetallic target by PLD. As a support we choose highly oriented pyrolytic graphite (HOPG) because it allows visualization of morphology of the deposited material by scanning probe microscopy. Furthermore, graphite is electrochemically inactive material so any electrochemical activity of the sample would be solely due to the presence of deposited metal. Our recent studies[30] of electrochemical activity of Au and Pt nanoparticles supported on HOPG surface and prepared by sublimation have demonstrated their low stability resulting from weak metal-HOPG interaction. It can be expected that nanoparticles prepared by PLD and originating from high temperature plasma will be more strongly anchored to the graphite surface and because PLD is the fast process the phase separation may not occur. In this communication we describe the results of XPS studies of Au-Pt nanostructures prepared by PLD. Selected samples were also studied by atomic force microscopy (AFM) method.

EXPERIMENTAL

Bimetallic material was deposited on highly oriented pyrolytic graphite (HOPG) provided by SPI Supplies, USA. The size of samples was 10 × 10 × 2 mm and the distance from the target approximately 40 mm. The clean surface of HOPG was obtained by peeling off few layers with an adhesive tape. The HOPG substrates were kept at room temperature during deposition. Prior to deposition, the surface of the target was cleaned by scraping by tungsten brush in preparation chamber of the spectrometer evacuated to a pressure better than 10^{-9} mbar. Ablation was carried out using Q-switched Nd:YAG laser (λ = 1064 nm, pulse width 6 ns, energy 60 mJ/pulse, repetition frequency 8 Hz) focused onto the target surface. The angle of radiation incidence was 50° from the sample surface. These conditions should ensure stoichiometric ablation and reasonable deposition times. The focused spot size determined by measuring the dimensions of the ablated region on the target after ~1000 pulses was approximately 0.60 mm^2. The attenuation of the laser beam intensity through Pyrex viewport was about 8% and heat dissipation due to the absorbed radiation did not represent a problem. Target used for ablation and containing nominally 75 wt.% Au and 25 wt.% Pt ($Au_{75}Pt_{25}$) was purchased from Research Institute for Metals (Panenské Břežany). The deposition was carried out under ultrahigh vacuum in the preparation chamber of the electron spectrometer. The used geometry is shown in Fig. 1. The sample was then transferred into the analyzer chamber of the spectrometer without contact with ambient atmosphere.

The XPS measurements were carried out using a VG ESCA3 MkII (VG Scientific, U.K.) electron spectrometer with a base pressure better than 10^{-10} mbar. AlKα radiation was used for excitation of electrons. Electrons were energy analyzed using a hemispherical analyzer operated at constant pass energy of 20 eV and giving an energy resolution, expressed by the FWHM of Au ($4f_{7/2}$) line, of 1.2 eV. The spectra of Pt (4f), Au (4f), C (1s) photoelectrons and C KLL X-ray excited Auger electrons were acquired. The spectra were recorded at room temperature. The overlapping spectral lines were resolved into individual components using the damped non-linear least squares method[31]. The estimated error in binding energy determination was ±0.1 eV.

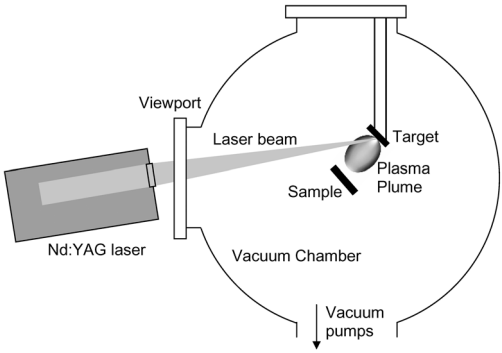

FIG. 1
Schematics of PLD experiment

The amounts of deposited metals are given in monolayer equivalents (MLE) as calculated from integrated intensities of Au (4f), Pt (4f) and C (1s) photoemission lines assuming Frank–van der Merwe (layer-by-layer) mode of growth (1 MLE (Au) = 1.52×10^{15} atoms cm^{-2}, 1 MLE (Pt) = 1.64×10^{15} atoms cm^{-2}). In these calculations theoretical values[32] of photoionization cross-sections and electron inelastic mean free paths values calculated from the TPP-2M equation[33] were used. In this way, the calculated number of metal monolayers, *m*, ranged from approximately 0.005 to 1. However, it is well known and also shown in this contribution that Au and Pt do not grow on HOPG in a layer-by-layer growth mode but due to their weak interaction with the support cluster formation is preferred. Consequently, the amounts of metals calculated from intensities of Au (4f), Pt (4f) and C (1s) core spectra are expected to be lower than the actual ones for clusters with size exceeding inelastic mean free path of electrons in Au or Pt (~1.65 nm). Comparison of the dependence of substrate core level photoemission intensity on photoemission intensity of the core level of deposited metal for different growth mechanisms is discussed in detail by Marcus[34]. Let us also to mention that the quartz crystal microbalance method often used for determination of the amount of the metal deposited gives as a rule higher amounts than actually deposited because of rather low (~0.1) sticking coefficient of metals on HOPG surface, particularly in the initial stages of deposition[35].

Morphology of the deposits was investigated using atomic force microscopy (AFM, Multimode Nanoscope IIIa, Veeco, U.S.A.) in the tapping mode. It should be noted that the AFM images shown here were measured *ex situ*.

RESULTS AND DISCUSSION

Figure 2 shows the spectra of Pt (4f) and Au (4f) photoelectrons taken from surface of the bimetallic target used for ablation. The ratio of atomic concentrations calculated from integrated intensities of the spectra was 6.0.

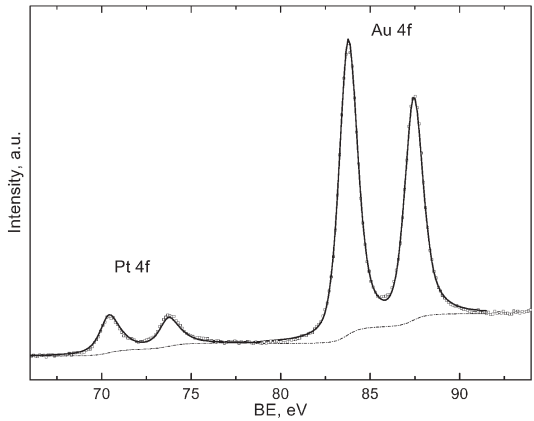

FIG. 2
Spectra of Pt (4f) and Au (4f) core electrons taken from $Au_{75}Pt_{25}$ bimetallic target (BE is the binding energy of electrons)

This result points to considerable segregation of gold in the near surface region which is likely due to its lower surface energy[36,37] compared to Pt. The measured binding energy of Au ($4f_{7/2}$) electrons coincided with value for pure gold (84.0 eV) while that obtained for Pt ($4f_{7/2}$) electrons (70.5 eV) was shifted downward by 0.6 eV. This shift agrees with value reported in literature[38] for Pt diluted in Au.

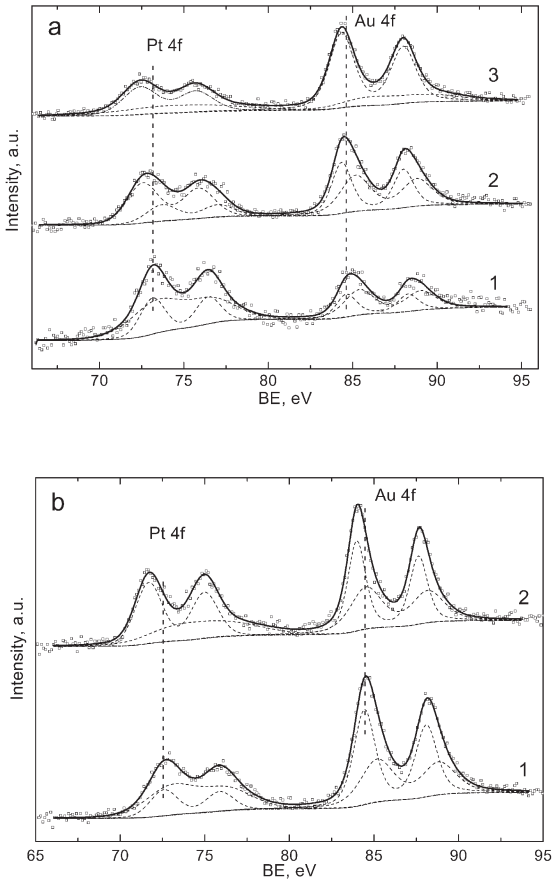

FIG. 3

Fitted spectra of Pt (4f) and Au (4f) core electrons taken from the nanodeposit on HOPG prepared from $Au_{75}Pt_{25}$ target cleaned by Ar^+ ion sputtering. a 1: 10 laser pulses, m(Au) = 0.005, m(Pt) = 0.01; 2: 30 pulses, m(Au) = 0.013, m(Pt) = 0.013; 3: 60 pulses, m(Au) = 0.032, m(Pt) = 0.017. b 1: 60 laser pulses, m(Au) = 0.032, m(Pt) = 0.017; 2: the same spectrum after heating the sample up to 300 °C for 1 h

In order to eliminate contamination of the deposited material the surface of the used target should be cleaned prior to deposition. Using standard procedure of Ar^+ ion sputtering resulted in target surface enrichment by Pt due to higher sputter yield of Au[39]. Consequently, if the target cleaned by ion sputtering was used for PLD then the composition of the produced nanodeposit as a function of laser fluence reflected concentration depth profile of Au and Pt in the target surface (Fig. 3a). Annealing of the deposit in vacuum resulted in decrease of both Au (4f) and Pt (4f) core level binding energies due to metal aggregation (Fig. 3b). At the same time Au/Pt atomic concentration ratio decreased from 1.82 to 1.27 due to mixing of metal atoms in the nanodeposit. To avoid complications with ion sputtered target we decided to clean the target *in situ* in the ultrahigh vacuum by mechanical scrapping using the tungsten brush. In this way the surface layer enriched by Au was also removed. Furthermore, before collecting the ablated material onto the HOPG substrate we applied 150 laser pulses to the target surface to achieve the stationary surface composition of ablated area.

The amounts of the deposited Au and Pt determined from integrated intensities of corresponding photoemission lines increased linearly with number of applied laser pulses. Ratio of atomic concentrations Au/Pt in the deposit was increasing with increasing laser fluence until the satura-

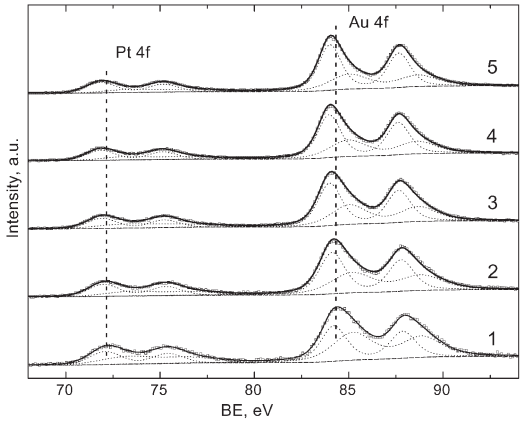

FIG. 4
Fitted spectra of Pt (4f) and Au (4f) core electrons taken from nanodeposits on HOPG prepared from $Au_{75}Pt_{25}$ target. 1: m(Au) = 0.088, m(Pt) = 0.031; 2: m(Au) = 0.186, m(Pt) = 0.055; 3: m(Au) = 0.280, m(Pt) = 0.074; 4: m(Au) = 0.377, m(Pt) = 0.097; 5: m(Au) = 0.457, m(Pt) = 0.121. The spectra are normalized to the same height

tion value 3.8 was achieved after approximately 200 laser pulses. The deposit was always enriched in Au. Annealing in vacuum or in 10^{-4} mbar of oxygen up to 500 °C resulted in increase of Au/Pt ratio due to surface segregation of Au.

Two components can be distinguished in the Au (4f) and Pt (4f) photoelectron spectra by curve fitting (Fig. 4). With increasing metal coverage the binding energies of the both components shift to lower values mainly because of increase of average size of nanoparticles. Binding energy of the high energy component is shifted relative to the low energy one by ~1 eV for Au (4f) and by ~1.5 eV for Pt (4f) spectrum. Intensity of the high energy component relative to the low energy one decreases with increasing surface coverage of HOPG by metals. We assign the lower binding energy component to metal nanoparticles and the higher binding energy peak to small clusters and/or metal atoms embedded in superficial layers of HOPG. The spectra of (4f) electrons thus reflect the presence of bimodal particle size distribution. Let us to mention that in this respect they are similar to the spectra of pure Au deposited by thermal evaporation on HOPG surface modified by argon ion sputtering[40]. The authors explain this result by existence of two types of adsorption sites with different adsorption energies.

Examination of size distribution of nanoparticles carried out by AFM (Fig. 5) revealed the presence of three maxima located at particles radii 75, 16 and 7 nm (Figs 5a, 5b), and with particle densities 2.4×10^7, 1.38×10^{10} and 1.45×10^{10} cm^2, respectively. It should be noted that due to the particle-tip convolution the size of nanoparticles is probably overestimated. The largest particles are likely due to the expulsion of droplets from the laser produced melt on the target surface and should exhibit bulk values of core level binding energies. Because of their very low population in the deposit they should not contribute significantly to the measured binding energies. We can thus attribute the presence of two doublets in the spectra of Au (4f) and Pt (4f) electrons to bimodal distribution of small nanoparticles (Fig. 5b).

It is now accepted that nucleation and growth of metallic particles on graphite surfaces is mainly governed by density of surface defects at which the nucleation takes place. There are three processes taking place on the HOPG surface which are related to energy of the impinging particles. Atoms which arrive with energy of a few eV can move on the surface until they are captured by defect site where they grow forming 3D clusters. There are also metal ions in a plasma plume with energies of the order of tens eV which can produce defect sites on the HOPG surface, induce resputtering and eventually may become implanted. Using the TRIM [41] Monte Carlo code we estimated the implantation depth Au^+ and Pt^+ ions with energy of 50 eV in

graphite as ~1 nm. Implanted ions thus remain within the depth measured by XPS. Formation of defects by impinging metal ions in superficial layers of HOPG should be accompanied by appearance of sp^3 hybridized carbon atoms. To this end we have measured carbon KLL Auger electron spectra of clean graphite surface and surface with 0.5 MLE of deposited metals. According to literature[42–45] one can estimate sp^2/sp^3 hybridization ratio using the energy separation between the most positive and the most negative excursions on the Auger C KLL derivative spectra. A linear relationship between this separation and population of sp^2 hybridized carbon atoms was proposed. In Fig. 6 the C KLL derivative spectra of clean HOPG surface and surface covered by 0.5 MLE of Au-Pt are displayed. For HOPG we obtained the separation 22.0 eV which is in good agreement with literature data[42–45].

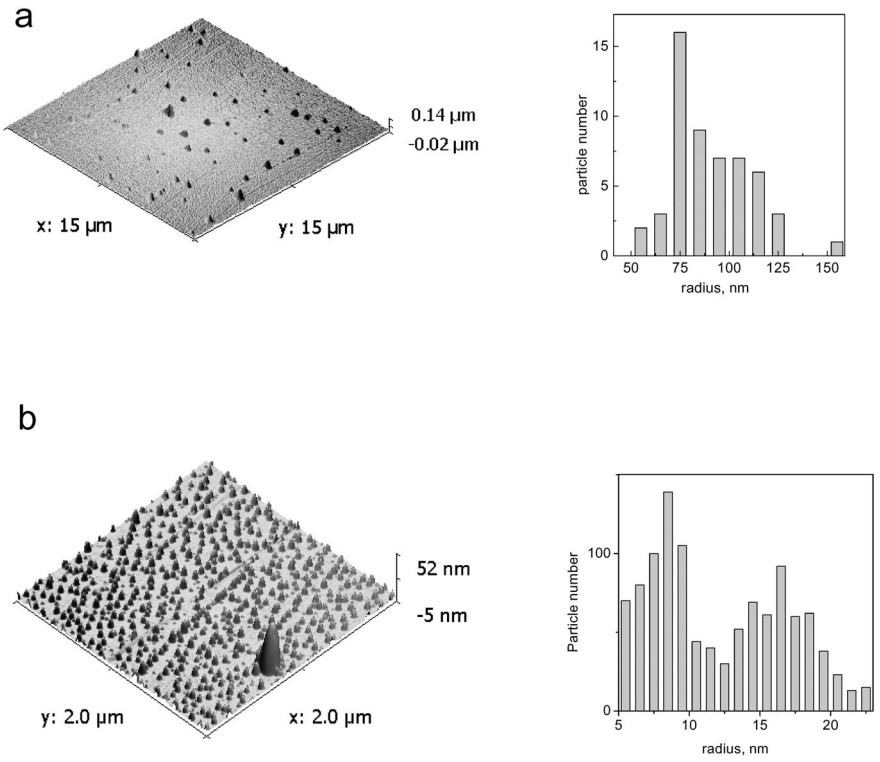

FIG. 5
AFM images of 0.1 MLE of Au-Pt nanodeposit on HOPG and histograms of number of nanoparticles versus their radius obtained from the analysis of AFM images

For clean HOPG sample with 0.5 MLE of deposited metals we got separation 18.0 eV which corresponds to presence of about 30% of sp^3 carbon atoms. PLD of metals results also in broadening of C (1s) photoemission line towards lower binding energy (Fig. 7). This broadening is caused by appear-

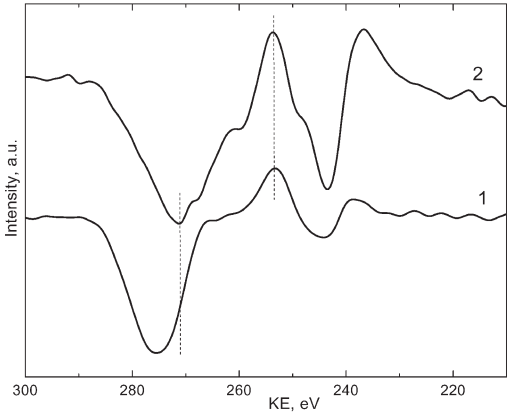

FIG. 6
C KLL X-ray excited derivative Auger spectra of 1: clean HOPG surface, 2: the same surface after pulsed laser deposition of 0.5 MLE of Au-Pt (KE is the kinetic energy of Auger electrons)

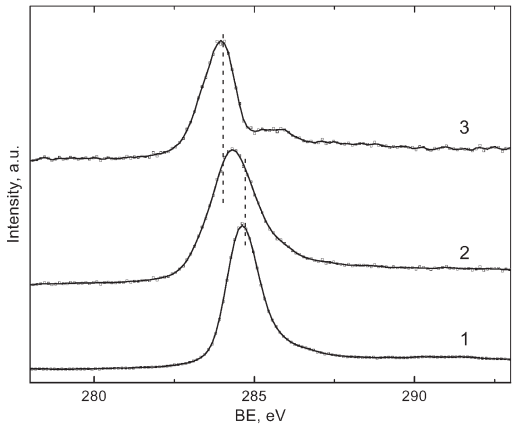

FIG. 7
Spectra of C (1s) electrons of 1: clean HOPG surface, 2: the same surface after pulsed laser deposition of ~1 MLE of Au-Pt, 3: the difference spectrum obtained by subtracting 1 from 2

ance of additional line induced by deposited metal and located at 283.8 eV. The intensity of this line increases with increasing amount of the deposited metal. We attribute it to the carbon atoms in contact with metal atoms. The electrons of the latter atoms can participate in relaxation process during photoemission of C (1s) core electrons and thus increase the relaxation energy and thereby decrease the binding energy.

The Au ($4f_{7/2}$) core level binding energy decreases with increasing metal surface coverage of HOPG substrate; for coverage 1×10^{-2} MLE the measured shift of the low binding energy component amounts ~0.5 eV with respect to bulk Au and is comparable to the shifts which we observed for pure Au clusters prepared by PLD on HOPG (Fig. 8.). However, this shift is lower than that we measured for Au deposited on amorphous carbon by conventional thermal evaporation. This result is in accord with assumption[40,46,47] that the surface defects act as nucleation centres for metal particles. On amorphous carbon the density of defects is significantly higher than on the basal plane of HOPG and consequently the higher density of smaller particles is present on amorphous graphite.

Shifts in the metal core-level binding energies to higher values with decreasing surface coverage by metal are characteristic of metals deposited on

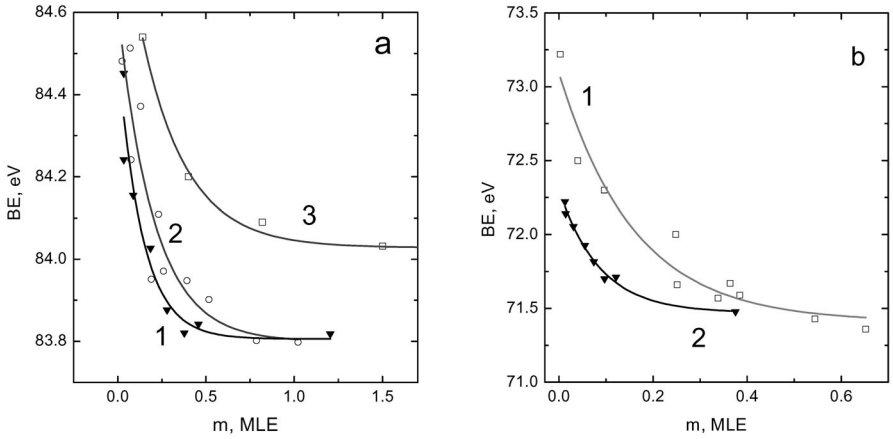

FIG. 8

Shift of the low binding energy component of Au ($4f_{7/2}$) core level spectra, BE, as a function of amount, *m*, of a: Au in 1: Au-Pt nanodeposit, 2: Au nanodeposit produced by PLD, 3: Au deposited on amorphous carbon by thermal evaporation (the spectra were fitted with one component only in this case) and of b: Pt in 1: Au-Pt nanodeposit, 2: Pt deposited on amorphous carbon surface by thermal vapour deposition

carbon surfaces[30,40,46–53]. The interpretation of these shifts is still controversial issue, in particular the contribution of initial and final state effects to the measured shifts. For understanding the dependence of core level binding energy on the particle size both, final and initial state effects should be taken into account. We believe that the final state effects due to Coulombic interaction of the outgoing photoelectron with positive hole remaining on the cluster and due to decreased extra-atomic relaxation dominate the measured shifts in laser deposited nanoparticles in the region of m(Au) < 0.2 MLE. When particle size increases the final state effects become less important and initial state effects come into play. For m(Au) > 0.2 MLE we observed that Au (4f) core levels of Au-Pt and Au deposited on HOPG are shifted with respect to the bulk value toward lower binding energy by 0.1–0.2 eV. This small negative shift cannot be explained by final state effects only. It is well known[54] that the Au (4f) electrons of Au surface atoms have binding energy lower by 0.4 eV than those of the bulk atoms. In small particles the proportion of surface atoms is higher than in the bulk counterpart and this could result in measured negative shift of the Au(4f) core level. Let us to mention that the negative shift of Au (4f) spectra was reported for Au-Pt bimetallic surface[55].

Qualitatively similar behaviour was observed for low binding energy component of Pt ($4f_{7/2}$) core level spectra. The size of the shift measured for low surface concentrations of Pt (~1×10^{-2} MLE) is by 1 eV lower than that obtained for Pt vapour deposited on basal plane of HOPG (Fig. 8b). It has been found[56] that vapour deposition of Pt on HOPG surface displaying few defect sites results in formation of large dendritic structures. In PLD the defects are produced by energetic ions and consequently formation of larger number of smaller clusters with higher values of core level binding energies for comparable amounts of deposited metal is expected. However, the measured values of Pt ($4f_{7/2}$) core level binding energy (Fig. 8b) for our Au-Pt nanodeposits are lower than those obtained for Pt deposited on pristine HOPG. The most likely interaction which could be responsible for the observed binding energy lowering is the interaction of Pt atoms with Au. It does not necessarily imply statistical distribution of Au and Pt atoms throughout the clusters. Formation of heteroaggregates or core-shell bimetallic structures in which Au and Pt are segregated is also possible. Further experiments have to be performed to study in more detail metal nucleation and growth in bimetallic deposits of immiscible metals prepared by PLD method. It should be mentioned that neither AFM nor XPS can yield direct information on chemical composition of individual particles and their surfaces. Electrochemical and adsorption experiments which can be helpful in

this respect are part of our on-going work aimed at understanding of electrochemical properties of bimetallic nanostructures prepared by PLD.

CONCLUSIONS

Supported Au-Pt nanostructures on HOPG surface have been prepared by PLD of bimetallic target. The nanoparticles prepared in this way were studied by XPS and AFM methods. The results of the both experimental methods consistently indicate presence of bimodal particle size distribution in the deposited nanostructures. The spectra of C KLL Auger electrons of HOPG surface with deposited metals point to formation of defects with sp^3 hybridized carbon atoms by impinging metal ions. The measured dependence of the Au (4f) core level binding energy on amount of Au in nanodeposit can be explained by combination of initial and final state effects in photoemission. On the basis of comparison of the dependence of Pt (4f) core level binding energy on amount of Pt present in the deposit with that obtained for Pt vapour deposited on basal plane of HOPG the presence of bimetallic nanostructures in the deposits prepared by PLD is suggested.

This work was supported by the Czech Science Foundation (Grant No. 104/08/1501) and by the Grant Agency of the Academy of Sciences of the Czech Republic (Grant No. 1ET400400413). The authors would also like to thank Dr. J. Franc for SEM images and EDX analyses of the bimetallic targets and Dr. I. Spirovova for technical assistance.

REFERENCES

1. Sinfelt J. H.: *Bimetallic Catalysts*. Wiley, New York 1983.
2. Ponec V., Bond G. C. in: *Studies in Surface Science and Catalysis* (B. Delmon and J. T. Yates, Eds), Vol. 95. Elsevier, Amsterdam 1995.
3. Ueda A., Haruta M.: *Gold Bull.* **1999**, *32*, 3.
4. Bond G. C., Thompson D. T.: *Gold Bull.* **2000**, 33, 41.
5. Valden M., Lai X., Goodman D. W.: *Science* **1998**, *281*, 1647.
6. Zhou S. H., Jackson G. S., Eichhorn B.: *Adv. Funct. Mater.* **2007**, *17*, 3099.
7. Zhou S. H., McIlwrath K., Jackson G., Eichhorn B.: *J. Am. Chem. Soc.* **2006**, *128*, 1780.
8. Zhong C. J., Maye M. M.: *Adv. Mater.* **2001**, *13*, 1507.
9. Mott D., Luo J., Smith A., Njoki P. N., Wang L., Zhong C. J.: *Nanoscale Res. Lett.* **2007**, *2*, 12.
10. Luo J., Njoki P. N., Mott D., Wang L., Zhong C. J.: *Langmuir* **2006**, *22*, 2892.
11. Luo J., Njoki P. N., Lin Y., Wang L., Zhong C. J.: *Electrochem. Commun.* **2006**, *8*, 581.
12. Sachtler J. W. A., Somorjai G. A.: *J. Catal.* **1983**, *81*, 77.
13. Hammer B., Morikawa Y., Nørskov J. K: *Phys. Rev. Lett.* **1996**, *76*, 2141.
14. Mihut C., Descorme C., Duprez C., Amiridis M. D.: *J. Catal.* **2002**, *212*, 125.

15. Luo J., Maye M. M., Petkov V., Kariuki N. N., Wang L., Njoki P., Mott D., Lin Y., Zhong C. J.: *Chem. Mater.* **2005**, *17*, 3086.
16. Xiao S., Hu W., Luo W., Wu Y., Li X., Deng H.: *Eur. Phys. J. B* **2006**, *54*, 479.
17. Adams R. D., Cotton F. A. (Eds): *Catalysis by Di- and Polynuclear Metal Cluster Complexes*. VCH Publishers Inc., New York 1997.
18. Xu J., Zhao T., Liang Z., Zhu L.: *Chem. Mater.* **2008**, *20*, 1688.
19. Crooks R. M., Zhao M. Q., Sun L., Chechik V., Yeung L. K.: *Acc. Chem. Res.* **2001**, *34*, 181.
20. Devarajan S., Bera P., Sampath S.: *J. Colloid Interface Sci.* **2005**, *290*, 117.
21. Zhou S., Jackson G. S., Eichhorn B.: *Adv. Funct. Mater.* **2007**, *17*, 3099.
22. Hamm G., Becker C., Henry C. R.: *Nanotechnology* **2006**, *17*, 1943.
23. Heemeier M., Carlsson A. F., Naschitzki M., Schmal M., Baumer M., Freund H.-J.: *Angew. Chem. Int. Ed.* **2002**, *41*, 4073.
24. Senkan S., Kahn M., Duan S., Ly A., Leidholm C.: *Catal. Today* **2006**, *117*, 291.
25. Abdelsayed V., Saoud K. M., El-Shall M. S.: *J. Nanoparticle Res.* **2006**, *8*, 519.
26. Yang Y., Saoud K. M., Abdelsayed V., Glaspell G., Deevi S., El-Shall M. S.: *Catal. Commun.* **2006**, *7*, 281.
27. Rousset J. L., Cadrot A. M., Lianos L., Renouprez A. J.: *Eur. Phys. J. D* **1999**, *9*, 425.
28. Eppler A. S., Rupprechter G., Guczi L., Somorjai G. A.: *J. Phys. Chem. B* **1997**, *101*, 9973.
29. Savastenko N., Volpp H.-R., Gerlach O., Strehlau W.: *J. Nanoparticle Res.* **2008**, *10*, 277.
30. Bastl Z., Franc J., Janda P., Pelouchová H., Samec Z.: *J. Electroanal. Chem.* **2007**, *605*, 31.
31. www.phy.cuhk.edu.hk/~surface/XPSPEAK
32. Scofield J. H.: *J. Electron Spectrosc. Relat. Phenom.* **1976**, *8*, 129.
33. Tanuma S., Powell C. J., Penn D. R.: *Surf. Interface Anal.* **1994**, *21*, 165.
34. Marcus P., Hinnen C.: *Surf. Sci.* **1997**, *392*, 134.
35. Arthur J. R., Cho A. Y.: *Surf. Sci.* **1973**, *36*, 641.
36. Vitos L., Ruban A. V., Skriver H. L., Kollar J.: *Surf. Sci.* **1998**, *411*, 186.
37. Wen Y.-N., Zhang J.-M.: *Solid State Commun.* **2007**, *144*, 163.
38. Hörnström S. E., Johansson L., Flodström A., Nyholm R., Schmidt-May J.: *Surf. Sci.* **1985**, *160*, 561.
39. http://www.npl.co.uk/server.php?show=ConWebDoc.605
40. Büttner M., Oelhafen P.: *Surf. Sci.* **2006**, *600*, 1170.
41. Ziegler J. F., Biersack J. P., Littmark U.: *The Stopping and Range of Ions in Solids*. Pergamon Press, New York 1985.
42. Galuska A. A., Maden H. H., Allred R. E.: *Appl. Surf. Sci.* **1998**, *32*, 253.
43. Lascovich J. M., Giorgi R., Scaglione S.: *Appl. Surf. Sci.* **1991**, *47*, 17.
44. Jackson S. T., Nuzzo R. G.: *Appl. Surf. Sci.* **1995**, *90*, 195.
45. Turgeon S., Paynter R. W.: *Thin Solid Films* **2001**, *394*, 44.
46. Fauth K., Heßler M., Batchelor D., Schütz G.: *Surf. Sci.* **2003**, *529*, 397.
47. Lopez-Salido I., Lim D. Ch., Dietsche R., Bertram N., Kim Y. D.: *J. Chem. Phys. B* **2006**, *110*, 1128.
48. Mason M. G.: *Phys. Rev. B* **1983**, *27*, 748.
49. Bastl Z.: *Vacuum* **1986**, *36*, 447
50. Ptáček P., Bastl Z.: *Appl. Surf. Sci.* **1990**, *45*, 319.
51. Mason M. G. in: *Cluster Models for Surface and Bulk Phenomena* (G. Pachcioni, Ed.). Plenum Press, New York 1992; and references therein.
52. Bastl Z.: *Collect. Czech. Chem. Commun.* **1995**, *60*, 383.

53. Richter B., Kuhlenbeck H., Freund H.-J., Bagus P. S.: *Phys. Rev. Lett.* **2004**, *93*, 026805.
54. Citrin P., Wertheim G. K., Baer Y.: *Phys. Rev.* **1983**, *27*, 3160.
55. Bastl Z., Pick Š.: *Surf. Sci.* **2004**, *566–568*, 832.
56. Howells A. R., Hung L., Chottiner G. S., Scherson D. A.: *Solid State Ionics* **2002**, *150*, 53.